ELSEVIER

Journal of Quantitative Spectroscopy & Radiative Transfer 103 (2007) 156–167

Journal of Quantitative Spectroscopy & Radiative Transfer

www.elsevier.com/locate/jqsrt

Amplitude and phase of light scattered by micro-scale aggregates of dielectric spheres: Comparison between theory and microwave analogy experiments

Pierre Sabouroux[a,b,*], Brian Stout[a,b], Jean Michel Geffrin[a,b], Christelle Eyraud[a,b], Isil Ayranci[c,d], Rodolphe Vaillon[c], Nevin Selçuk[d]

[a]*Institut Fresnel, UMRCNRS 6133, Université de Provence, Aix-Marseille 1, France*
[b]*Université Paul Cézanne, Aix-Marseille 3, Ecole Généraliste d'Ingénieurs de Marseille, Campus de Saint Jérôme, Case 162, 13397 Marseille Cedex 20, France*
[c]*Centre de Thermique de Lyon (CETHIL CNRS-INSA Lyon-UCBL), INSA de Lyon, 69621 Villeurbanne, France*
[d]*Chemical Engineering Department, Middle East Technical University, 06531 Ankara, Turkey*

Received 18 April 2006; received in revised form 1 June 2006; accepted 2 June 2006

Abstract

Light scattering is a useful diagnostic tool for characterization of particles. Direct scattering measurements for arbitrarily shaped micro-scale particles is difficult due to small-scale limitations. Microwave analogy is a convenient approach to realize such measurements as it enables realization of analogous experiments with larger model particles in a spectral domain where wavelengths are on centimeter scale. In the present study a test model analogous to light scattering by a micro-scale aggregate of dielectric spheres was constructed and experimentally characterized in the microwave regime. Measured amplitude and phase of the scattered field were compared with theoretical predictions obtained from quasi-exact multiple-scattering T-matrix method and discrete dipole approximation (DDA). Excellent agreement demonstrates the validities of both the experiment and the models.

Keywords: Aggregate; Dielectric sphere; Microwave; Scattering; T-matrix method; DDA method; Microwave analogy

0. Introduction

For a long time now the interaction between electromagnetic waves and small solid aggregate-forming particles (dust, flakes, grains pollens, etc.) has generated a number of questions due to the complexity of the problem. Despite considerable efforts and progress, the difficulty of the problem is underlined by the comparatively small number and quality of quantitative experimental results.

The majority of experimental studies on such aggregates involves optical diagnostics. However, in order to validate the theoretical modeling of these light–particle interactions, it is essential to have a precise knowledge

*Corresponding author. Tel.: +33 4 91 28 83 53; fax: +33 4 91 67 67 44 28.
E-mail address: pierre.sabouroux@fresnel.fr (P. Sabouroux).

0022-4073/$ - see front matter © 2006 Elsevier Ltd. All rights reserved.
doi:10.1016/j.jqsrt.2006.06.001

of the geometry and constitution of the aggregates. Since the characteristic dimensions of such particles in the optical domain is often of the same order of magnitude as the wavelength of light, the particles are too small to conveniently allow the fabrication of aggregates with precisely controlled geometries. Given these obstacles to such studies, one practical solution is to simultaneously scale both the characteristic dimensions of the aggregate and the wavelength of the incident radiation so that they are both on the centimeter scale. This method was employed in the 1970s for determination of the radar equivalent surface of aeronautical vehicles [1] and characterization of interplanetary dust grains [2].

In this work, we propose to use such techniques to study the interaction of electromagnetic waves with a complex shape particle such as a small size aggregate of spheres. Indeed, micro-scale aggregates constitute a class of particles, which are of interest in astrophysics (interstellar grains) and in mechanical and chemical engineering (soot particles) to cite a few examples. In the particular case of combustion products such as soot, characterization from optical diagnostics can permit a better understanding of their formation processes and then enable proposals of methods to reduce their production and thereby limit pollution. In any case, non-intrusive or remote sensing optical techniques based on the measurement and analysis of light scattered by these micro-sized particles are classically employed. However, to better understand the results of optical measurements new methods using electromagnetic waves with much larger wavelengths and scaling allows comparative studies to be carried out on model aggregates of considerably larger size. The characteristic particle dimensions in the present study are on the centimeter scale. Gustafson and his co-workers [3–8] employed a similar methodology. However, use was made of millimetric wavelengths (about 3 mm), which can hinder a precise characterization and/or the fabrication of certain test aggregates. The utilization of lower frequencies allows measurements to be carried out on rigorously controlled geometries.

On the other hand, a scattered field is completely characterized by its intensity, polarization state and phase and hence complete validation of electromagnetic scattering models necessitates experimental data on both amplitude and phase of the scattered field at two orthogonal polarization states. To the authors' knowledge such complete data was not previously published for dielectric agglomerates. Experimental data presented in this study is expected to be useful for validation of scattering models in terms of all primary variables.

This article is presented in three distinct parts. In the first part, the measurement apparatus and the model aggregate employed here are presented. In the second part, two models are presented for calculating the light scattered by the aggregate when subject to an incident electromagnetic field. In the third part, model predictions are compared with experimental results and conclusive remarks are made. Then, we present our conclusions and future works.

1. Description of the model aggregate and the experimental apparatus.

This first part presents the model dielectric aggregate and the microwave frequency experimental apparatus used in this study.

1.1. Model aggregate

As pointed out in the introduction, the characteristic size of the test aggregate (Fig. 1) is linked to the wavelength characterizing the incident electromagnetic wave so that the target (i.e. the aggregate) is of comparable size. The wavelength of the incident radiation can vary between 1.7 cm (18 GHz) and 15 cm (2 GHz). The apparatus making up the measurement chain determines this frequency range. The chosen material is an optically transparent dielectric, which aids in optimizing the alignments of the experimental configuration thanks to the utilization of laser beam. At the present time, the precision of the target position is inferior to 1 mm or in other words $\lambda/20$ for the highest encountered frequencies which is the most extreme case.

The global geometry of the aggregate is cubic. The aggregate is composed of a collection of 27 dielectric spheres each having a diameter of $D = 15.90 \pm 0.05$ mm. The edge of a cube is therefore 47.7 mm long. The spheres are composed of a PMMA (Altuglass, Fig. 2) with a relative permittivity of 2.5. This value was measured with the aid of a device developed in our laboratory: *EpsiMu* [9].

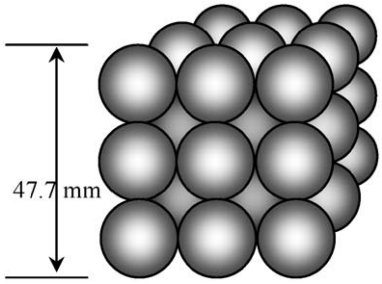

Fig. 1. Aggregate schematic.

Fig. 2. Photo of the test aggregate.

The wavelength utilized has to be compared to the dimension of an edge of the cube containing the 27 dielectric spheres. We choose then as a geometric parameter for comparison, kw where $w = 3 \times D$ represents the edge of the cube, i.e. 47.7 mm. In this manner $kw = 2\pi w/\lambda$.

1.2. Experimental apparatus

The experimental system is composed of a collection of mechanical positioners set within an anechoic chamber. Absorbers are HYFRAL APM66 and the reflectivity is less than –50 dB from 3 to 20 GHz. The internal dimensions of the chamber are 14.50 m long, 6.50 m wide and 6.50 m high. The mechanical positioners enable the emission and reception antennas follow circular trajectories centered on target to be analyzed. In the present case, the target aggregate is positioned at the center of these circular trajectories with an expanded polystyrene mast. The rigourous alignment of the target in the middle of the chamber is realised with a laser beam. The distance between the origin and the antennas is 173.50 cm for the emitting antenna and 175 cm for the receiving antenna.

The trajectories of the emission and reception antennas are contained in a horizontal plane passing through the center of the spherical coordinate system describing the setup. Two incident field directions are studied: a "face incidence" for which the propagation direction is perpendicular to one of the faces of the cube (case 0°), and an "edge incidence" for which the beam is oriented at an angle of 45° with respect to the normal (case 45°) as shown in Figs. 3 and 4. Furthermore, two incident field polarizations are studied with respect to the bistatic plane, i.e. the plane containing both the incident wave vector $\mathbf{k}_i$, and the scattered wave vector $\mathbf{k}_r \equiv k\hat{\mathbf{r}}$ where $\hat{\mathbf{r}}$ is the detector direction). "Vertical polarization" represents the case where electric field is normal to the bistatic plane, and "horizontal polarization" is used when the electric field lies within the bistatic plane (sometimes referred to as "parallel" to the bistatic plane).

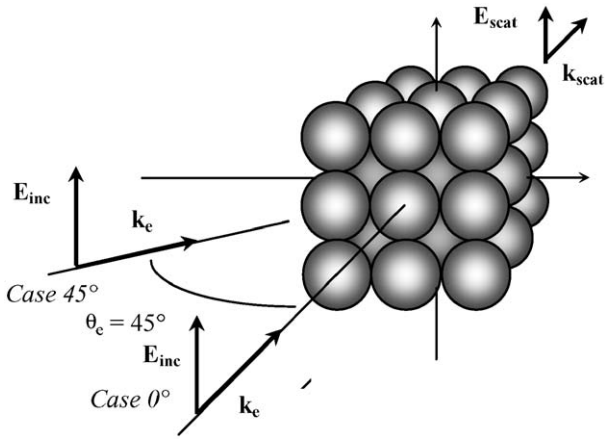

Fig. 3. Studied geometries.

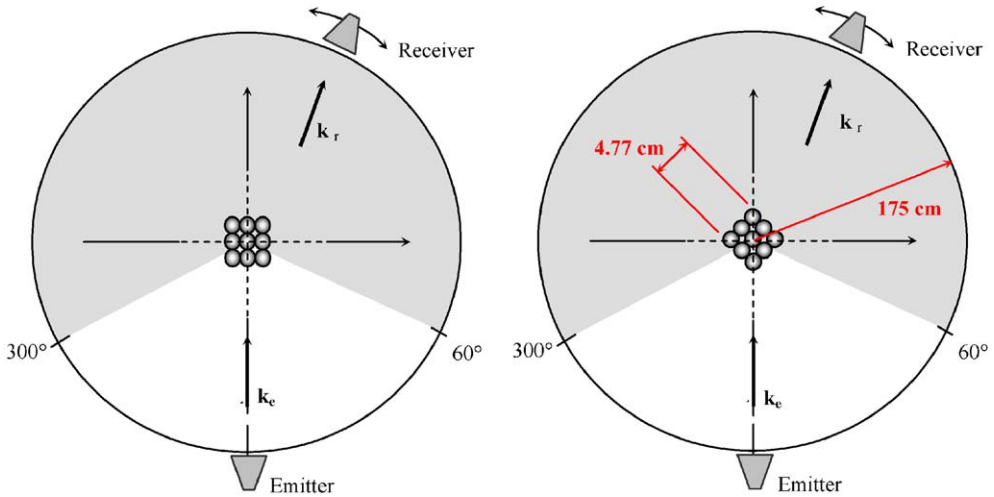

Fig. 4. Geometric disposition of the two positions of the aggregate with respect to the incident field. Case 0° on the left and Case 45° on the right.

The experimental setup has already been described in the reference papers [10–11]. The electromagnetic wave is emitted by a large band horn type antenna, designated as *double ridged antenna linearly polarized* (ARA DRG 118A). The incident polarization is fixed by the orientation of the emission antenna. The reception antenna is oriented such that the principal polarization is measured. The domain of angular detection covers 60–300° with the direction of forward scattering being designated by 180°. The angular step size is fixed to 1°. The microwave detection setup employs a vector network analyzer (HP8510C) working with multiple sources and mixers displaced and brought to the level of the antennas in order to limit the measurement uncertainties arising from the considerable length of the coaxial cables.

The measurement protocol, as described in Refs. [10–11], allows us to obtain both the amplitude and phase of the electric field scattered by the target (i.e. the aggregate). The scattered field is obtained by vector subtraction of the electromagnetic field with and without the presence of the target. The first of these two measurements corresponds to the total field measured with the target in place, which corresponds to a superposition of the incident and scattered fields. The second measurement is simply that of the incident field measured with the target removed. Under these conditions, for each frequency, and for each angular position,

the value of the complex diffracted field is the result of the vector subtraction of incident field (without the target) from the total field (with the target).

2. Theoretical calculations

2.1. Amplitude scattering matrix or S-matrix

We begin by defining a scattering plane as the plane containing the incident wave vector and the direction vector of the detector. If the incident field can be approximated by a plane wave in the region of the target, then it can be expressed as

$$\begin{aligned}\mathbf{E}_{\mathrm{i}} &= (E_{0//,\mathrm{i}}\hat{\mathbf{e}}_{//,\mathrm{i}} + E_{0\perp,\mathrm{i}}\hat{\mathbf{e}}_{\perp,\mathrm{i}})\exp(\mathrm{i}kz - \mathrm{i}\omega t)\\ &= E_{//,\mathrm{i}}\hat{\mathbf{e}}_{//,\mathrm{i}} + E_{\perp,\mathrm{i}}\hat{\mathbf{e}}_{\perp,\mathrm{i}},\end{aligned} \tag{1}$$

where $k \equiv 2\pi/\lambda$, $E_{0//,\mathrm{i}}, E_{0\perp,\mathrm{i}}$ are complex constants, and $\hat{\mathbf{e}}_{//,\mathrm{i}}$ and $\hat{\mathbf{e}}_{\perp,\mathrm{i}}$ are unit vectors which are, respectively, parallel and perpendicular to the scattering plane, and chosen so that $(\hat{\mathbf{e}}_{//,\mathrm{i}}, \hat{\mathbf{e}}_{\perp,\mathrm{i}}, \hat{\mathbf{k}}_{\mathrm{i}})$ form a right-handed coordinate system.

Denoting the detector direction $\hat{\mathbf{k}}_{\mathrm{s}}$, the far-field limit of the scattered field will have a spherical wave-type behavior in the neighborhood of the detector

$$\begin{aligned}\mathbf{E}_{\mathrm{s}} &\cong (E_{0//,\mathrm{s}}\hat{\mathbf{e}}_{//,\mathrm{s}} + E_{0\perp,\mathrm{s}}\hat{\mathbf{e}}_{\perp,\mathrm{s}})\frac{\exp(\mathrm{i}kr - \mathrm{i}\omega t)}{-\mathrm{i}kr}\\ &= (E_{//,\mathrm{s}}\hat{\mathbf{e}}_{//,\mathrm{s}} + E_{\perp,\mathrm{s}}\hat{\mathbf{e}}_{\perp,\mathrm{s}}),\end{aligned} \tag{2}$$

where the $-\mathrm{i}k$ factor in the denominator is a (non-universal) historical convention. The complex amplitudes $E_{0//,\mathrm{s}}$ and $E_{0//,\mathrm{s}}$ are functions of the detector angle, and the unit vectors $(\hat{\mathbf{e}}_{//,\mathrm{s}}, \hat{\mathbf{e}}_{\perp,\mathrm{s}}, \hat{\mathbf{k}}_{\mathrm{s}})$ form a right-handed coordinate system.

Adopting a coordinate system in which the $\hat{\mathbf{k}}_{\mathrm{i}}$ direction defines the $\hat{\mathbf{z}}$ axis, the $\exp(\mathrm{i}\mathbf{k}_{\mathrm{i}} \cdot \mathbf{r})$ becomes simply $\exp(\mathrm{i}kz)$, and the relationship between the $E_{//,\mathrm{s}}, E_{\perp,\mathrm{s}}$ and the incident field components, $E_{//,\mathrm{i}}, E_{\perp,\mathrm{i}}$ can be expressed via a 2×2 amplitude scattering matrix S [12]:

$$\lim_{r\to\infty}\begin{bmatrix} E_{//,\mathrm{s}} \\ E_{\perp,\mathrm{s}} \end{bmatrix} = \frac{\exp(\mathrm{i}k(r-z))}{-\mathrm{i}kr}\begin{bmatrix} S_2 & S_3 \\ S_4 & S_1 \end{bmatrix}\begin{bmatrix} E_{//,\mathrm{i}} \\ E_{\perp,\mathrm{i}} \end{bmatrix}, \tag{3}$$

where r and z are the length of the detector arm and the emitter to target distance, respectively and are equivalent in the present configuration. Each of the four scattering matrix elements in (S_1, S_2, S_3, S_4), are functions of the "scattering angle" θ, and the "azimuthal angle" ϕ [12].

Amplitude and phase of the scattered field, which are the parameters of interest, can be obtained from the elements of the amplitude scattering matrix. Complex constants of the incident and scattered electric fields in (1) and (2) can be represented in phasor notation as

$$E_{//,\mathrm{i}} = \mathrm{a}_{//,\mathrm{i}}.\exp(\mathrm{i}\delta_{//,\mathrm{i}}), \quad E_{\perp,\mathrm{i}} = \mathrm{a}_{\perp,\mathrm{i}}.\exp(\mathrm{i}\delta_{\perp,\mathrm{i}}), \tag{4}$$

$$E_{//,\mathrm{s}} = \mathrm{a}_{//,\mathrm{s}}.\exp(\mathrm{i}\delta_{//,\mathrm{s}}), \quad E_{\perp,\mathrm{s}} = \mathrm{a}_{\perp,\mathrm{s}}.\exp(\mathrm{i}\delta_{\perp,\mathrm{s}}). \tag{5}$$

Amplitude scattering matrix elements are complex numbers that can also be expressed in the form

$$S_n = |S_n|.\mathrm{e}^{\mathrm{i}\delta_n} \quad n = 1, 2, 3, 4. \tag{6}$$

The ratio of amplitude of scattered wave in the far field to that of incident wave can be obtained by substituting Eqs. (4–6) in Eq. (3) and rearranging:

$$M_{//,//} = \frac{a_{//,\mathrm{s}}}{a_{//,\mathrm{i}}} = \frac{|S_2|}{kr}, \tag{7}$$

$$M_{\perp,\perp} = \frac{a_{\perp,\mathrm{s}}}{a_{\perp,\mathrm{i}}} = \frac{|S_1|}{kr}. \tag{8}$$

Similarly, the phase difference between the scattered and incident fields can be obtained as

$$\Delta\phi_{//,//} = -\left[\delta_2 - \frac{\pi}{2}\right], \tag{9}$$

$$\Delta\phi_{\perp,\perp} = -\left[\delta_1 - \frac{\pi}{2}\right]. \tag{10}$$

2.2. T-Matrix calculations

When an object (aggregate) is composed of a number of components, one can obtain an essentially exact solution to the scattering fields by coupling a multiple-scattering theory of finite clusters with the T-matrices of the component objects [13–15]. When the components of the aggregate are spheres, the T-matrices of the individual spheres have analytic expressions obtained through generalizations of Mie theory [16]. Although any near or far-field information can be obtained from the T-matrix formulation that we employ, we are concerned herein only with far-field applications.

The principal difficulties encountered in the past for such T-matrix treatments were in the formulation of numerically reliable T-matrix computation schemes. Nowadays, numerical stability is no longer an obstacle since it can be overcome in a variety of ways (stable recursive algorithms, fast iterative schemes, sparse matrix inversions, etc.). In particular, numerical instabilities in the *stable* recursive RCTMA algorithm [13,14] employed here (*not* to be confused with earlier *unstable* recursive algorithms [17]) have not been observed to date [13–15,19–21]. The only other difficulty encountered is the necessity of generating the required special functions in efficient computer codes, but this problem has been successfully addressed in recent decades.

2.2.1. Extraction of the amplitude scattering matrix from the T-matrix

One requires the derivation of appropriate formulas in order to pass from the more complete scattering information residing within a system T-matrix [13–15] to the more limited scattering information described by the amplitude scattering matrix S. The comparison with experiment is facilitated by fixing the $\hat{\mathbf{x}}$-axis to be some readily identifiable direction in the experimental setup (we chose the $\hat{\mathbf{x}}$-axis to define the "vertical" direction in the experimental setup).

With the above coordinate system choices one can analytically calculate a set of incident field coefficients for each of the possible polarizations $a_{//}$ and $a_{\perp}$ [14,15]:

$$\begin{aligned} a_{//,q,v,\mu} &= i^{v+1}\sqrt{\pi(2v+1)}[\delta_{\mu,1}e^{-i\phi} - (-)^q\delta_{\mu,-1}e^{-i\phi}], \\ a_{\perp,q,v,\mu} &= i^{v}\sqrt{\pi(2v+1)}[\delta_{\mu,1}e^{-i\phi} + (-)^q\delta_{\mu,-1}e^{-i\phi}], \end{aligned} \tag{11}$$

where $0 \leqslant \phi \leqslant (\pi/2)$ is the azimuthal angle between the scattering plane and the $\hat{\mathbf{x}}$-axis (for e.g. $\phi = \pi/2$ for all comparisons with experiments illustrated in this work).

The indices in Eq. (11) are associated with the fact that these coefficients correspond to different types of electromagnetic partial waves composing the incident field. The $v = 1, \ldots, N_{\max}$ are a multipole index with $N_{\max}$ being a truncation parameter which usually determines the precision of the calculation to about the same order as the Mie theory of a single spherical particle. In Eq. (11), we also remark an angular momentum projection index $\mu = -n, \ldots, n$ and a wave-type index $q = 1, 2$ where $q = 1$ designates waves generated from magnetic "sources" and $q = 2$ from electric sources [15,18]. The physical meaning of the indices can however be ignored at this point, however, since the physics of the electromagnetic waves has already been addressed when deriving Eqs. (3) and (11–14).

The next step in calculating the S-matrix is to construct a set of scattering coefficients $f^{(j)}_{//,p,n,m}$ and $f^{(j)}_{\perp,p,n,m}$ for each of the $j = 1, \ldots, N$ particles in the aggregate by matrix multiplication of the block matrices, $\tau_N^{(j,k)}$, composing the full body-centered T-matrix, τ_N, and the incident coefficients $a_{//}$, $a_{\perp}$ given above [13–15]:

$$f^{(j)}_{//,p,n,m} = \sum_{k=1}^{N}\sum_{q=1,2}\sum_{v,\mu}\exp(ik\hat{\mathbf{z}}\cdot\mathbf{x}_k)[\tau_N^{(j,k)}]_{p,n,m;q,v,\mu}a_{//,q,v,\mu} \tag{12}$$

and idem for the perpendicular polarization, $\perp$. Once these calculations have been carried out, one can readily calculate the S-matrix components from the following analytical formulae:

$$
\begin{aligned}
S_1 &= \sum_{j=1}^{N} \exp(-\mathrm{i}\mathbf{k}_s \cdot \mathbf{x}_j) \sum_{n,m} \exp(\mathrm{i}m\phi)\mathrm{i}^{-n} \\
&\quad \times [\vec{s}_n^m(\cos\,\theta) f^{(j)}_{\perp,1,n,m} + \vec{u}_n^m(\cos\,\theta) f^{(j)}_{\perp,2,n,m}], \\
S_4 &= \sum_{j=1}^{N} \exp(-\mathrm{i}\mathbf{k}_s \cdot \mathbf{x}_j) \sum_{n,m} \exp(\mathrm{i}m\phi) i^{-n} \\
&\quad \times [\vec{s}_n^m(\cos\,\theta) f^{(j)}_{//,1,n,m} + \vec{u}_n^m(\cos\,\theta) f^{(j)}_{//,2,n,m}], \\
S_2 &= -\sum_{j=1}^{N} \exp(-\mathrm{i}\mathbf{k}_s \cdot \mathbf{x}_j) \sum_{n,m} \exp(\mathrm{i}m\phi)\mathrm{i}^{-n+1} \\
&\quad \times [\vec{u}_n^m(\cos\theta) f^{(j)}_{//,1,n,m} + \vec{s}_n^m(\cos\,\theta) f^{(j)}_{//,2,n,m}], \\
S_3 &= -\sum_{j=1}^{N} \exp(-\mathrm{i}\mathbf{k}_s \cdot \mathbf{x}_j) \sum_{n,m} \exp(\mathrm{i}m\phi)\mathrm{i}^{-n+1} \\
&\quad \times [\vec{u}_n^m(\cos\,\theta) f^{(j)}_{\perp,1,n,m} + \vec{s}_n^m(\cos\,\theta) f^{(j)}_{\perp,2,n,m}],
\end{aligned} \tag{13}
$$

where $\mathbf{k}_s = (\omega/c)\hat{\mathbf{k}}_s$. The $\cos\,\theta$-dependent functions, $\vec{u}_n^m$ and $\vec{s}_n^m$, in Eq. (13) are obtained from the associated Legendre functions:

$$
\begin{aligned}
\vec{u}_n^m(\cos\,\theta) &\equiv \gamma_{nm} \frac{im}{\sin\theta} P_n^m(\cos\,\theta), \\
\vec{s}_n^m(\cos\,\theta) &\equiv \gamma_{nm} \frac{d}{d\theta} P_n^m(\cos\,\theta), \\
\gamma_{nm} &\equiv \left(\frac{(2n+1)(n-m)!}{4\pi n(n+1)(n+m)!} \right)^{1/2}.
\end{aligned} \tag{14}
$$

2.3. Discrete Dipole Approximation

Discrete Dipole Approximation (DDA) is a well-established approach for estimation of scattering and absorption of electromagnetic radiation by arbitrarily shaped particles of size comparable to incident wavelength. This approach is categorized as one of the volume-integral equation methods for numerical modeling of electromagnetic scattering [22]. Pioneered by Purcell and Pennypacker [23], DDA has been improved to its present state mostly by Draine and Flatau [24,25]. The approximation is based on replacement of a continuum real scatterer by a finite array of interacting discrete dipoles positioned at the sites of a lattice such that the lattice spacing is small compared to wavelength. The oscillating polarizations (dipole moments) induced on each dipole due to the incident wave and the electric fields of the other oscillating dipoles in the system can be expressed by linear relations depending on polarizability of the dipole, incident electric field, positions and polarizations of other dipoles. The resulting system of $3N$ coupled linear equations, N being the total number of dipoles, represents a discrete analog of the integral equation that governs the scattering problem. Once the system of complex linear equations is solved for polarizations, the scattered electric fields at desired scattering planes and directions can be readily evaluated. The associated formulations for evaluation of polarizations, forward scattering amplitude matrix elements, amplitude scattering matrix elements, absorption emission and scattering cross sections were extensively documented previously [24].

Publicly available DDSCAT code [26] developed by Draine and Flatau provides a flexible means for application of DDA methodology. The code was previously developed and validated for estimation of scattering and absorption by irregular targets in terms of radiative properties such as scattering and

absorption cross sections, some of the 4×4 scattering matrix elements, etc. ([27] and references cited therein) which are parameters that characterize polarization state and intensity of the scattered field and are eventually related to the magnitudes of the amplitude scattering matrix elements. However, for prediction of phase, some modifications related to the position of dipoles with respect to origin of the scattering plane needs to be incorporated into the most recent code (v.6.1) so that the arguments of the complex scattering matrix elements can be predicted correctly. Details of prediction of amplitude and phase of the scattered field by using DDSCAT can be found in [28] where the accuracy of the modified code was demonstrated on single sphere targets of various sizes and materials by validating both the magnitudes and phases of the predicted complex amplitude scattering matrix elements against Mie theory solutions.

The target of 27-sphere cubic agglomerate under consideration was framed in a $48 \times 48 \times 48$ cubic lattice in which the number of occupied lattice sites amount to 56781 dipoles. This discretization with $|m|kd = 0.27$ for 8 GHz case and $|m|kd = 0.47$ for 14 GHz case was checked to satisfy the applicability criterion of DDSCAT, reported as $|m|kd < 0.5$, where m represents the complex index of refraction and d stands for the lattice spacing [26,27]. DDSCAT code modified for phase computations [28] was run by using the target shape module for multisphere targets (NSPHER), generalized prime factor algorithm for fast Fourier transform (GPFAFT), preconditioned biconjugate gradient method with stabilization (PBCGST) for iterative solution of the system of complex linear equations and corrected lattice dispersion relation by Gutkowitcz–Krusin and Draine (GKDLDR) for determination of dipole polarizabilities. Error tolerance used in conjugate gradients method was 10^{-5}. Resulting amplitude scattering matrix elements were substituted in Eqs. (6–10) to obtain amplitude and phase of scattered field relative to the incident field.

3. Results, comparison between theory and experiment

Due to the large volume of experimental data gathered from our test aggregate composed of 27 spheres in a cubic arrangement, we choose two representative frequencies and compare the results: 8 GHz ($\lambda = 3.75$ cm) and 14 GHz ($\lambda = 2.14$ cm). We have then two values for the kw parameter, $w = 3 \times D$ indicative of aggregates whose total size are far from being small with respect to the wavelength:

$$\text{For } f = 8\,\text{GHz}, \quad \lambda = 3.75\,\text{cm} \rightarrow kw = 8,$$

$$\text{For } f = 14\,\text{GHz}, \quad \lambda = 2.14\,\text{cm} \quad \rightarrow kw = 14.$$

In order to compare results between theory and experiment, a normalization is performed. For the amplitudes, we simply normalize with respect to the scattering maximum of forward scattering. The phase is similarly normalized by taking forward scattering to define the origin of the phase shift.

Comparison between experimental and theoretical results for the cases of polarization parallel and perpendicular to the scattering plane when the incident wave vector was normal to the face of an aggregate (case 0°) are illustrated in Figs. 5a–d. Analogous results obtained for an incident wave vector oriented along an edge of the cube are grouped in Figs. 6a–d. In both figures, the experimental results are embodied by a solid black curve. The theoretical results generated by the multiple scattering T-matrix method are represented by a solid gray curve. Finally, the results obtained from the DDSCAT method are illustrated by using black crosses. As can be seen from the figures, theoretical and experimental results are in excellent agreement.

We observe some slight differences in the phase curves at the two frequencies for the case of incidence on the face of the target (case 0°). This is apparently due to a slight misalignment of the target in the experimental reference frame.

In view of the excellent agreements, we can now consider our experimental protocols to be validated as well as our means for carrying out theoretical modeling via the T-matrix or DDA. Under these conditions, we are currently planning the characterizations of more realistic aggregates containing larger number of particles in more complex configurations where absorption is present.

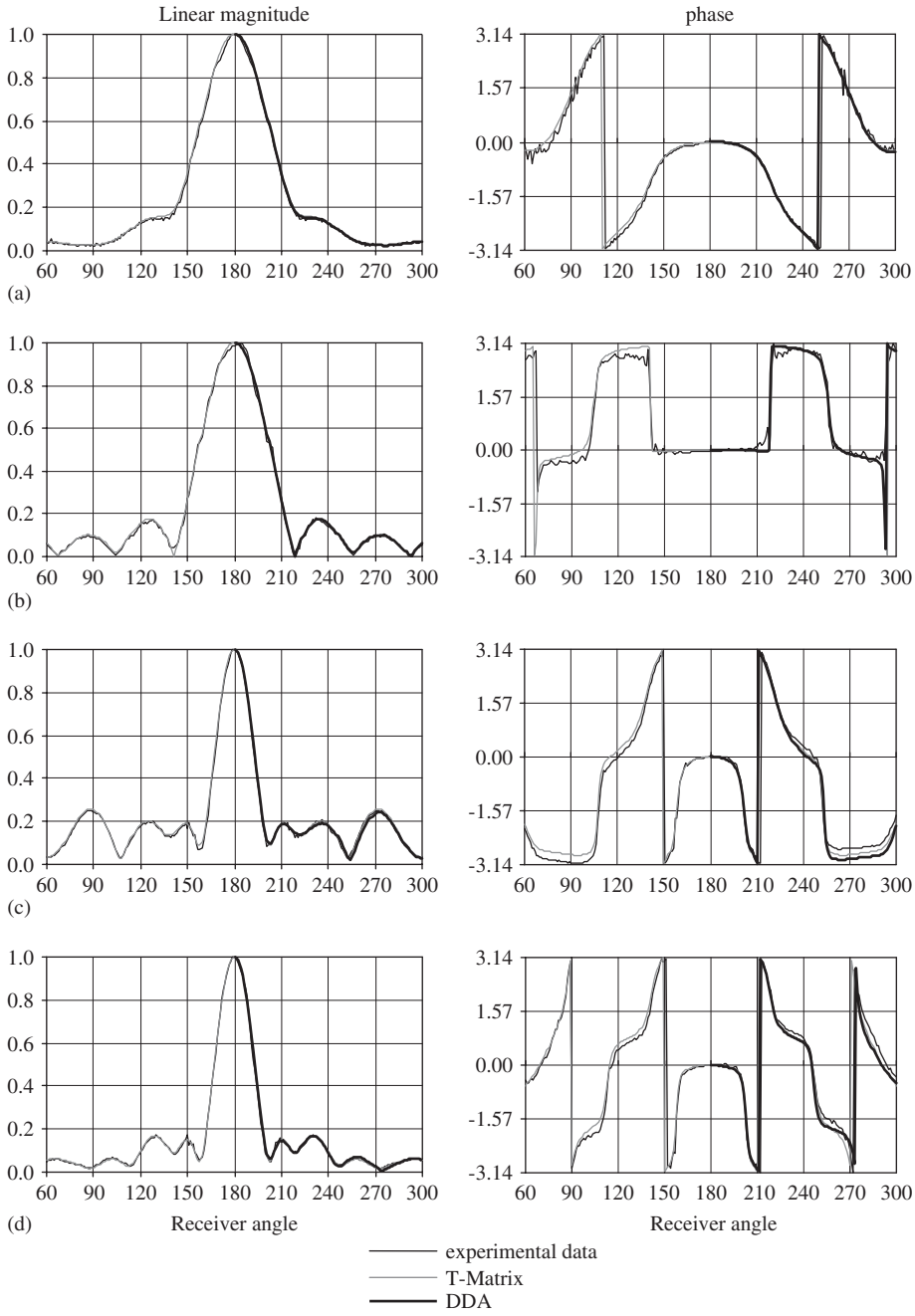

Fig. 5. (a) Case 0°: polarisation //, 8 GHz; (b) Case 0°: polarisation ⊥, 8 GHz (c) Case 0°: polarisation //, 14 GHz; (d) Case 0°: polarisation ⊥, 14 GHz.

4. Conclusions

Electromagnetic scattering of light by microscale aggregates of dielectric spheres has been investigated both theoretically and experimentally. Magnitude and phase of scattered field measured by microwave analogy principle were compared with predictions of T-Matrix and DDA models. The originality of those measurements is that both magnitude and phase are measured.

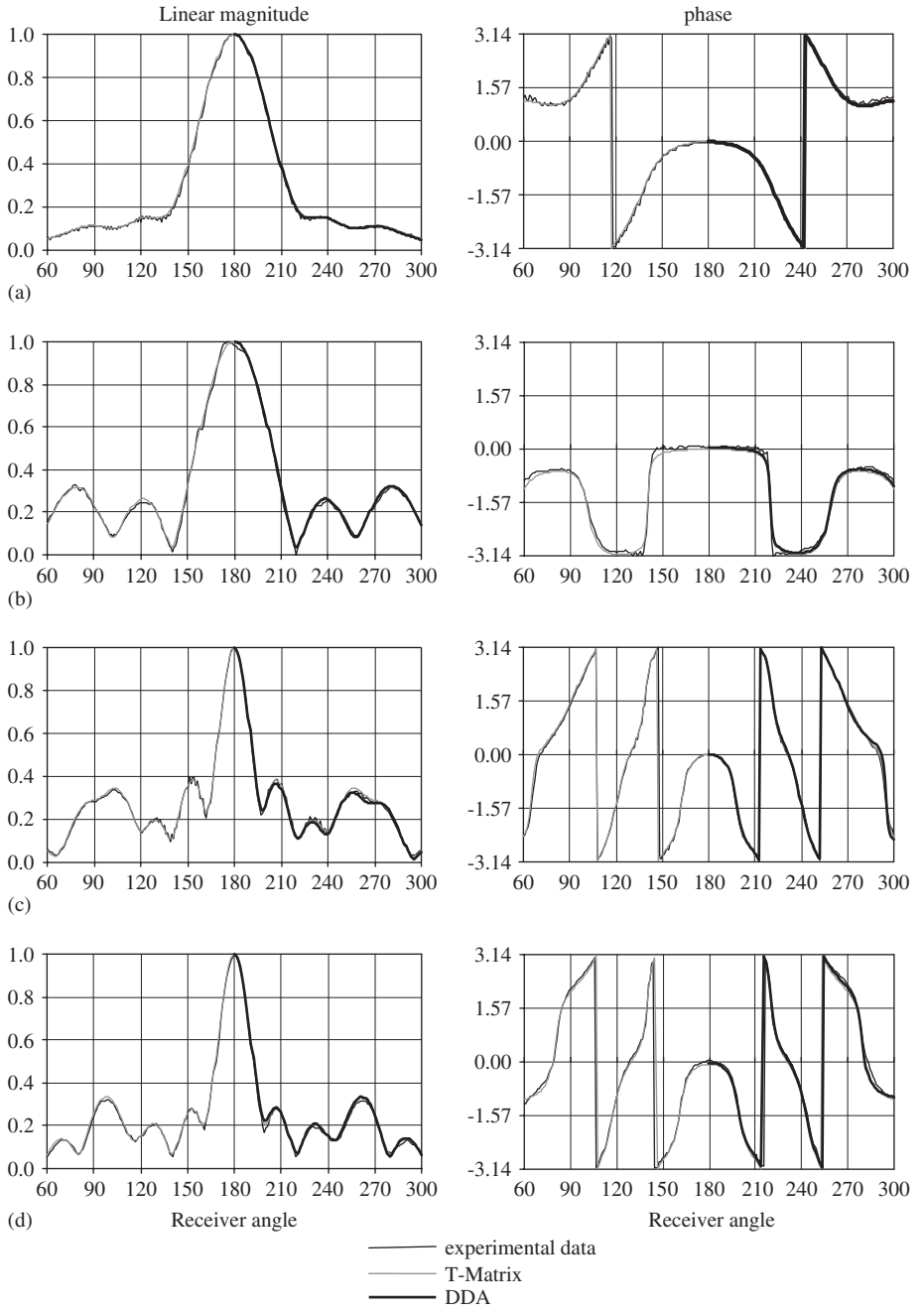

Fig. 6. (a) Case 45°: polarisation //, 8 GHz; (b) Case 45°: polarisation ⊥, 8 GHz; (c) Case 45°: polarisation //, 14 GHz; (d) Case 45°: polarisation ⊥, 14 GHz.

Excellent agreements between the model predictions and measurements reveal the validity of both the experimental approach and the models for analysis of electromagnetic scattering in similar situation. The experimental data presented here provide reference solutions against which light scattering models can be tested for accurate prediction of both amplitude and phase of scattered fields.

As future work, it is planned to extend the analysis to chain-like aggregates of absorbing spheres. Morphology and optical properties will be selected so as to be representative of soot particles produced by

reactive media. The interest of this work, associating experimental measurements and different types of theoretical modeling calculations on aggregates of spheres, should also manifest itself in the astrophysical community for studies concerning interstellar dust. Indeed, some stellar dust grains are also assumed to have the shape of aggregates.

Experimental data are available electronically on request to the corresponding author.

Acknowledgments

The authors of the DDSCAT code, Bruce T. Draine and Piotr J. Flatau, are gratefully acknowledged. This study was partially supported by the French Ministry of Research (Réseau de Recherche et d'Innovation Technologique: ''Recherche Aéronautique sur le Supersonique'', decision no. 03T233) and by Turkish Scientific and Technical Research Council (TÜBİTAK) with project no. MİSAG-263. Işıl Ayrancı was supported by a French Government Scholarship granted by the Embassy of France in Turkey within the frame of a joint Ph.D. program co-supervised by METU and INSA de Lyon.

References

[1] Crispin JW, Siegel KM. Method of radar cross-section analysis. Electrical science series. New York: Academic Press; 1968.
[2] Greenberg JM, Pedersen NE, Pedersen JC. Microwave analog to the scattering of light by nonspherical particles. J Appl Phys 1961;32:233–42.
[3] Gustafson B. Microwave analog to light scattering measurements: a modern implementation of a proven method to achieve precise control. JQSRT 1996;55(5):663–72.
[4] Xu Y, Gustafson BÅS. A generalized multiparticle Mie-solution: further experimental verification. JQSRT 2001;70(4–6):395–419.
[5] Gustafson BÅS. Scattering by simple and complex systems I: methods. In: Greenberg JM, Li A, editors. Formation and evolution of solids in space, vol. 523. Dordrecht: Kluwer Academic Publishers; 1999. p. 535–48.
[6] Gustafson BÅS, Kolokolova L, Thomas-Osip JE, Waldemarsson KWT, Loesel J, Xu Y-l. Scattering by simple and complex systems II: microwave measurements. In: Greenberg JM, Li A, editors. Formation and evolution of solids in space. Dordrecht: Kluwer Academic Publishers; 1999. p. 549–63.
[7] Gustafson BS. Microwave analog to light scattering measurements. In: Mishchenko MI, Hovenier JW, Travis LD, editors. Light scattering by nonspherical particles: theory, measurements, and geophysical applications. New York: Academic Press; 1999. p. 367–90 [ISBN 0-12-498660-9, Chapter 13].
[8] Xu Y-l. Electromagnetic scattering by an aggregate of spheres: far field. Appl Opt 1997;36:9496–508.
[9] Sabouroux P, Boschi P. EpsiMu un nouvel outil pour déterminer les caractéristiques électromagnétiques de matériaux dans le domaine des hyperfréquences. Rev Electr Electron 2005;10:58–62.
[10] Belkebir K, Bonnard S, Pezin F, Sabouroux P, Saillard M. Validation of 2D inverse scattering algorithms from multi-frequency experimental data. J Electromagn Waves Appl 2000;14:1637–67.
[11] Geffrin JM, Sabouroux P, Eyraud C. Free space experimental scattering database continuation: experimental set-up and measurement precision. Inverse Probl 2005;21:S117–30.
[12] Bohren CF, Huffmann ER. Absorption and scattering of light by small particles. New York: Wiley; 1983.
[13] Stout B, Auger JC, Lafait J. A transfer matrix approach to local field calculations in multiple scattering problems. J Mod Opt 2002;49:2129–52.
[14] Auger JC, Stout B. A recursive T-matrix algorithm to solve the multiple scattering equation: numerical validation. JQSRT 2003;79–80:533–47.
[15] Stout B, Auger JC, Lafait J. Individual and aggregate scattering matrices and cross sections: conservation laws and reciprocity. J Mod Opt 2001;48(14):2105–28.
[16] Tsang L, Kong J, Shin R. Theory of microwave remote sensing, Wiley series in remote sensing. New York: Wiley; 1985.
[17] Siqueira PR, Sarabandi K. T-matrix determination of effective permittivity for three-dimensional dense random media. IEEE Trans Antennas Propagat 2000;48.
[18] Jackson JD. Classical electrodynamics, 3rd ed. New York: Wiley; 1999.
[19] Auger JC, Stout B, Martinez V. Scattering efficiency of aggregated clusters of spheres: dependence on configuration and composition. JOSA A 2005;22:2700–8.
[20] Stout B, Andraud C, Stout S, Lafait J. Absorption in multiple scattering systems of coated spheres. JOSA A 2003;20:1050–9.
[21] de Silva A, Andraud C, Charron E, Stout B, Lafait J. Multiple light scattering in multistratified media: model experiment. Physica B 2003;338:74–8.
[22] Kahnert FM. Numerical methods in electromagnetic scattering theory. JQSRT 2003;79:775–824.
[23] Purcell EM, Pennypacker CR. Scattering and absorption of light by nonspherical dielectric grains. Astrophys J 1973;186:705–14.
[24] Draine BT. The discrete-dipole approximation and its application to interstellar graphite grains. Astrophys J 1988;333:848–72.

[25] Draine BT, Flatau PJ. Discrete-dipole approximation for scattering calculations. J Opt Soc Am A—Opt Image Sci Vis 1994;11: 1491–9.
[26] Draine BT, Flatau PJ. User guide for the discrete dipole approximation code DDSCAT.6.1, 2004. 〈http://arxiv.org/abs/astro-ph/0409262〉.
[27] Draine BT. The discrete dipole approximation for light scattering by irregular targets. In: Mishchenko MI, Hovenier JW, Travis LD, editors. Light scattering by nonspherical particles: theory, measurements and applications. San Diego: Academic Press; 2000. p. 131–45.
[28] Ayranci I, Vaillon R, Selçuk N. Performance of discrete dipole approximation for prediction of amplitude and phase of electromagnetic scattering by particles. JQSRT 2006, in press, doi:10.1016/j.jqsrt.2006.06.006.